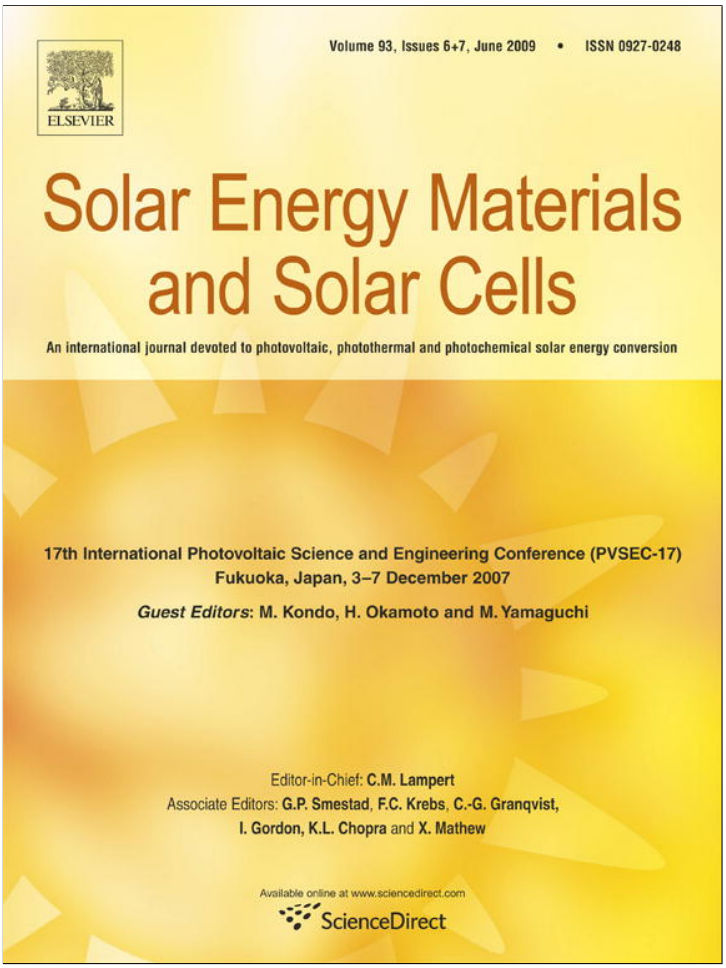

Solar Energy Materials & Solar Cells 93 (2009) 952–957

Contents lists available at ScienceDirect

Solar Energy Materials & Solar Cells

journal homepage: www.elsevier.com/locate/solmat

Hybrid poly (3-hexylthiophene)/titanium dioxide nanorods material for solar cell applications

Tsung-Wei Zeng, Hsi-Hsing Lo, Chia-Hao Chang, Yun-Yue Lin, Chun-Wei Chen, Wei-Fang Su *

Department of Materials Science and Engineering, National Taiwan University, 1, Roosevelt Road, Section 4, Taipei 106-17, Taiwan

ARTICLE INFO

Article history:
Received 14 December 2007
Accepted 21 November 2008
Available online 9 January 2009

Keywords:
Titanium dioxide
Nanorod
Poly(3-hexylthiophene)
Solar cell
Hybrid
Kelvin probe force microscopy

ABSTRACT

We conducted an extensive study on poly(3-hexylthiophene) (P3HT) in combination with titanium dioxide (TiO_2) nanorods hybrid material for polymer solar cell applications. The device performance critically depends on the morphology of the hybrid film that will be determined by the molecular weight of P3HT, the solvent type, the hybrid compositions, the surface ligand on the TiO_2 nanorods, film thickness, process conditions, and so on. The current–voltage characteristic of the device fabricated in air has shown a power conversion efficiency of 0.83% under air mass (AM) 1.5 illumination using high molecular weight (65,000 D) P3HT, high boiling point solvent trichlorobenzene, and pyridine-modified TiO_2 nanorods with a film thickness of about 100 nm. The Kelvin probe force microscopy (KPFM) study of hybrid films shows large-scale phase separation with domain size greater than 10 nm, which may be the main factor limiting device performance.

1. Introduction

Conjugated polymers are of great interest for the production of low-cost and flexible photovoltaic cells. The development of the interpenetrating electron donor–acceptor conjugated polymer-based bulk heterojunction devices, such as polymer:fullerene [1,2], polymer:polymer [3], and polymer:nanocrystal [4–6], in the last decade, has made it possible to reach high photovoltaic conversion.

The metal oxides offer high physical and chemical stability, and thus have been widely studied as a material for polymer photovoltaic conversion [7–9]. For the conjugated polymer and titanium dioxide (TiO_2) hybrid solar cells, two main approaches have been developed [10], filling thin films of nanostructured TiO_2 with conjugated polymers to produce photovoltaic cells [7,11–15] or randomly mixing the polymer and the TiO_2 nanocrystal to fabricate polymer hybrid solar cells [16,17]. The one-dimensional semiconductor TiO_2 nanorods are selected as an electron acceptor in this study for offering direct pathways for electric conduction in polymer solar cells. The photoinduced charge transfer of hybrid MEH-PPV and TiO_2 nanorods has been reported [18,19]. The MEH-PPV:TiO_2 nanorods hybrid has been used as an active material for photoconversion [17,18]. Here, we were interested in using a high-mobility polymer, poly(3-hexylthiophene) (P3HT), in combination with TiO_2 nanorods to obtain solution-processed bulk heterojunction solar cells. The device performance was found to critically depend on the material properties and processing conditions. Kelvin probe force microscopy (KPFM) was introduced to investigate the polymer:nanocrystal hybrid material bi-continuous phase. KPFM allows measuring the structural and electronic properties of organic thin films [20,21].

2. Experimental details

Synthesis of the TiO_2 nanorod end-capped by oleic acid (OLEA) was performed according to the method reported in the literature [22]. Details and results have been described in an earlier work [17]. Because the ligand can act as a potential barrier for charge transfer, we removed the original OLEA ligand according to the literature with some modifications [23]. The as-synthesized OLEA end-capped TiO_2 nanorods were dispersed in pyridine and left under stirring at 70 °C until the solution turned clear. Later, the treated nanocrystals were then washed with hexane and isolated by centrifuging, and redispersed in pyridine. Thermogravimetric analysis was used to confirm that a large fraction of oleic acid was removed through the procedures.

The indium-tin-oxide (ITO)/poly (3,4-ethylenedioxythiophene)–poly (styrenesulfonate) (PEDOT: PSS)/P3HT:TiO_2 nanorods/TiO_2 nanorods/Al device was fabricated in the following manner: ITO glass substrate (15 Ω/□, Merck) was ultrasonically cleaned in a series of organic solvents (ethanol, methanol, and acetone). A 60-nm-thick layer of PEDOT:PSS (Aldrich) was spin-cast onto the ITO substrate, followed by baking at 120 °C for 20 min. Typically, the hybrid P3HT:TiO_2 nanorods (47 wt%:53 wt%) films

* Corresponding author. Tel./fax: +886 2 33664078.
E-mail address: suwf@ntu.edu.tw (W.-F. Su).

0927-0248/$ - see front matter © 2008 Elsevier B.V. All rights reserved.
doi:10.1016/j.solmat.2008.11.023

were first prepared from a mixed coating solutions of TiO_2 nanorods in dichloromethane:pyridine (5:1/vol:vol) and P3HT in trichlorobenzene (TCB), followed by coating a pure TiO_2 nanorods layer (~30 nm) from its pyridine solution. The thickness of the active layer was controlled by the concentration of the solutions. Then, the 120 nm Al electrode was vacuum deposited on top of the device.

The film thickness was determined by α-stepper (DEKTAK). The current–voltage characterization (*I–V*) (Keithley 2400 source meter) was performed under 10^{-3} Torr vacuum, with air mass (AM) 1.5 or monochromatic illumination at defined devices area (Oriel Instruments). The AM 1.5 condition (100 mW/cm^2) has been calibrated using a standard silicon solar cell. A 400 nm cutoff filter was used to remove the UV light. The P3HT:TiO_2 films were cast on a glass plate to obtain UV–visible transmittance (Jasco V-570). Time-resolved photoluminescence (TRPL) spectroscopy was performed with a time-correlated single-photon-counting spectrometer (Picoquant, Inc.). A pulse laser (375 nm) with a duration of 70 ps operating at 40 MHz was used for excitation. Thick films for the time of flight (TOF) measurement are prepared by drop-casting the P3HT/TiO_2 nanorods blend solutions on the glass substrates precoated with semitransparent aluminum electrodes (35 nm) by thermal evaporation at a vacuum about 10^{-6} Torr. The film thickness is ranged from 1.5 to 3.0 μm. The measured samples are then completed by the thermal evaporation of thicker aluminum cathodes (~200 nm) through a shadow mask. For the TOF transient photocurrent measurement, a thin layer of charge carriers is generated under illumination through the semitransparent electrode using a frequency-tripled Nd:YAG-pulsed laser ($\lambda = 355$ μm). Under the applied electric field, these carriers drift towards the counter electrode, giving the transient photocurrent signal recorded by a digital oscilloscope (Tetronix TDS5052B). KPFM and topography were recorded in the darkness using the lift mode. The first scan recorded the topographic signal, then a second scan, following the topography acquired in the first scan, recorded the surface potential signal using a silicon cantilever with Pt surface coating (Digital Instruments Nanoscope III).

3. Results and discussion

The TOF hole mobilities in thick films of P3HT showed the influence of number-average molecular weight (Mw) on hole mobility (Table 1). The TOF mobility measurements were performed in a similar way according to the literature [24]. The hole mobility for Mw = 65,000 D (65k) P3HT is more than three times than that of P3HT Mw = 10k. Absorption spectra for various Mw P3HT films are shown in Fig. 1. We observe a blue shift for low Mw film as compared with the high Mw film. The blue shift is attributed to the decrease in the effective conjugation length that comes from the finite size confinement effects of the small molecules [25].

For the hybrid film, as TiO_2 nanorods incorporated into the P3HT (50 wt%:50 wt%), the presence of photoinduced charge transfer at the P3HT/TiO_2 nanorods interfaces can be evident from TRPL spectroscopy as shown in Fig. 2. The OLEA end-capped TiO_2 nanorods invoke a slight reduction of photoluminescence

Table 1
The hole mobility of P3HT with different molecular weights.

P3HT's Mw (D)	Applied *E*-field (V/cm)	Hole mobility (cm^2/V/s)
10k	4.65×10^5	0.66×10^{-4}
30k	4.64×10^5	1.49×10^{-4}
66k	4.41×10^5	2.14×10^{-4}

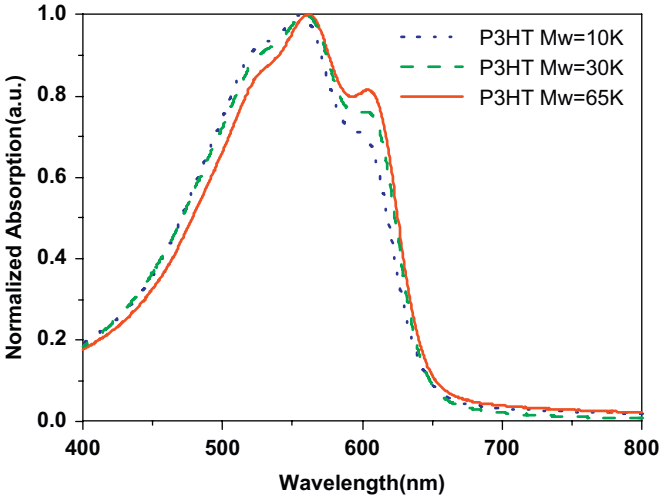

Fig. 1. Absorption spectra for various Mw films spin-cast from TCB.

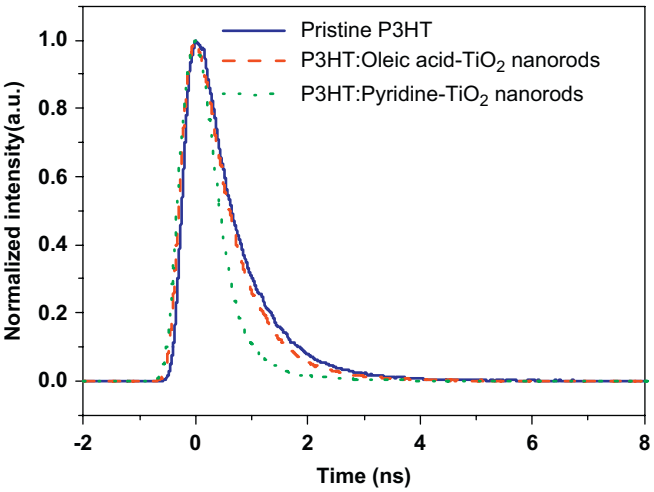

Fig. 2. Photoluminescence lifetime decay of P3HT:TiO_2 nanorods hybrid as compared with pristine P3HT.

(PL) lifetime. The presence of a new non-radiative process for photogenerated excitons is an evidence of the charge separation taking place at the interface between the polymer and TiO_2 nanorods [19]. After we performed pyridine treatment to remove most of the surfactant on the TiO_2 surface, the pyridine-treated TiO_2 nanorods in the P3HT resulted in a more pronounced reduction in PL lifetime, indicating the insulating surface ligand, OLEA, might act as a barrier for charge separation. Thus, the pyridine-treated TiO_2 nanorods were selected as the acceptor in this study.

The photovoltaic devices fabricated have a configuration as shown in Fig. 3. The TiO_2 nanorod thin film can serve as a hole-blocking electron-transporting layer in the photovoltaic devices [17]. We made devices going from 20 to 60 wt% TiO_2 nanorod in the P3HT:TiO_2 nanorods hybrid. The maximum short-circuit current (J_{sc}) was found for the 53 wt%:47 wt% TiO_2 nanorods: P3HT composite.

Effect of Mw of P3HT was studied via a comparison of finished devices. The *I–V* curve characteristics show that the short-circuit density increases with the Mw of P3HT (Fig. 4). This can be attributed to the improvement in hole mobility. TCB, which has a high boiling point, was selected as a solvent, for P3HT crystallites can be formed during a longer time available for the polymer

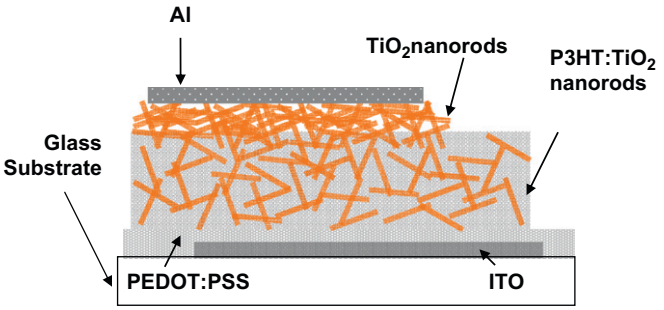

Fig. 3. Schematic structure of P3HT:TiO_2 nanorods hybrid solar cells.

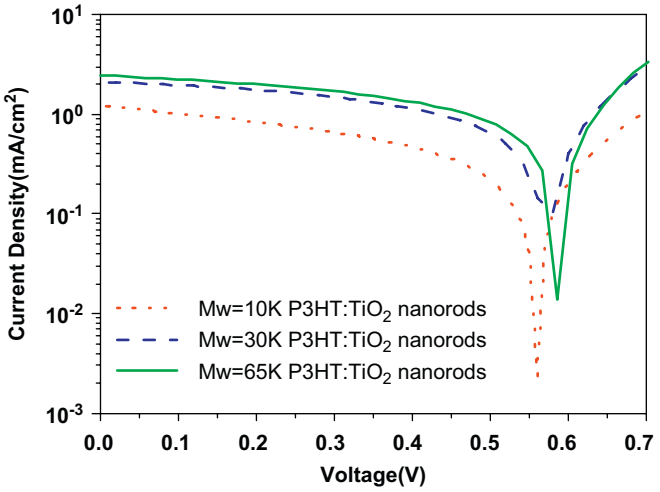

Fig. 4. The plot of current density as the function of applied voltage for different devices made of various P3HT molecular weights.

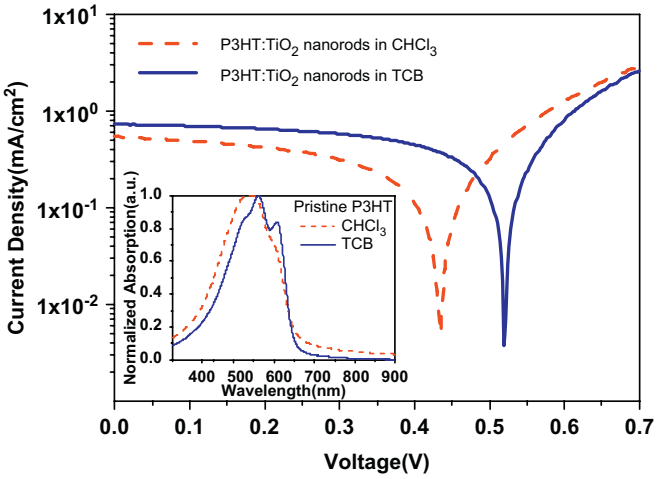

Fig. 5. The plot of current density as the function of applied voltage for different devices made with different solvents.

chains in solution to crystallize. As the solvent was replaced by chloroform, lowered device performance was observed (Fig. 5). This can be explained by comparing the absorption spectra of the P3HT thin film cast from chloroform compared with that cast from TCB (Fig. 5 inset). The blue-shifted spectrum evidences the P3HT molecule within the film, forming a twisted, disordered structure cast from chloroform. The less-obvious shoulder at 600 nm in the absorption spectrum was observed from the film

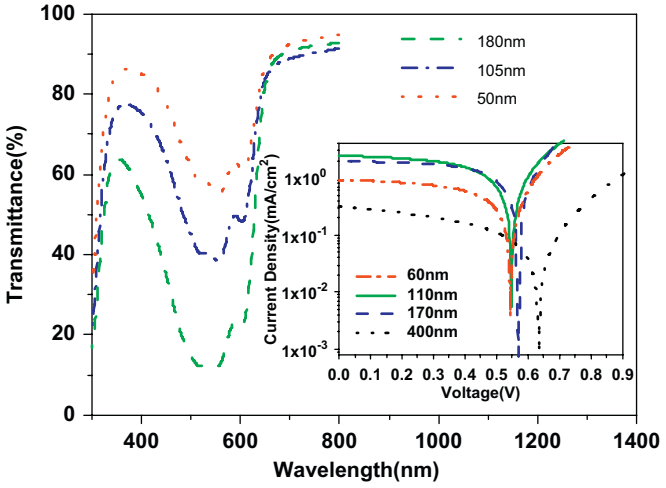

Fig. 6. Transmittance spectra of P3HT:TiO_2 nanorods hybrid materials for various film thicknesses. The inset shows the plots of current density as the function of applied voltage for different devices having different film thickness.

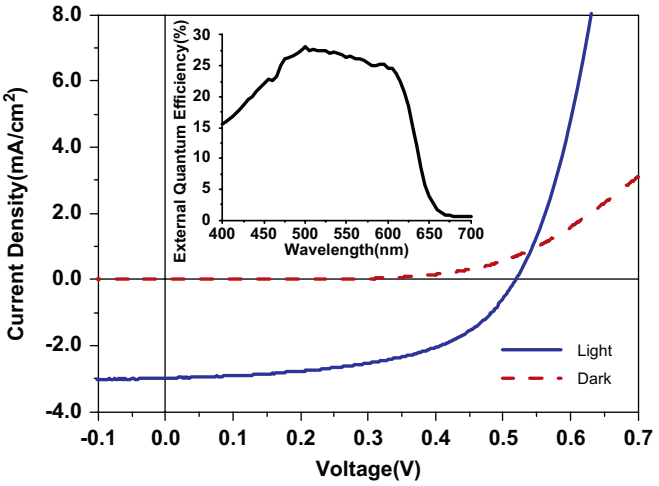

Fig. 7. The corresponding *I–V* curves from the optimized device at AM 1.5 illumination (100 mW/cm^2). The inset shows the external quantum efficiency for the device.

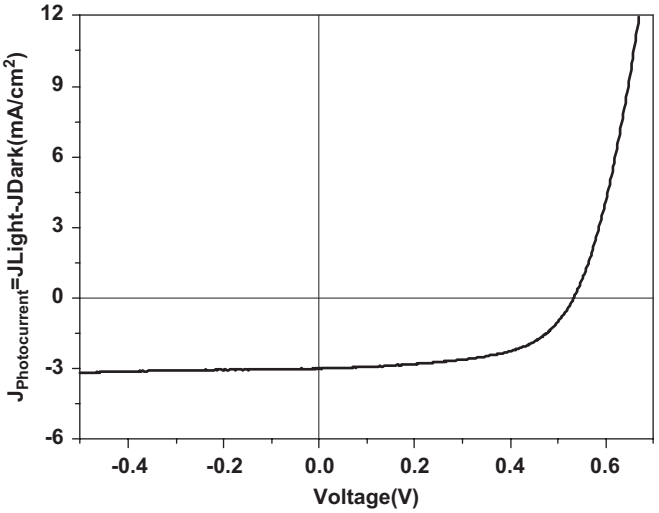

Fig. 8. The photocurrent of the optimized device as a function of applied bias. (The photocurrent is the difference in the current between under illumination and in the dark.)

cast by chloroform, indicating that the P3HT chain inter-plane stacking was less pronounced in this case. The shoulder at 600 nm has been assigned to P3HT inter-plane interactions [26]. The less-well-resolved structure in the spectrum cast from chloroform can be attributed to the relatively wider distribution of conjugation lengths.

Fig. 6 shows the transmittance spectra or the fraction of incident light absorbed by P3HT as a function of wavelength for several different P3HT:TiO_2 nanorods film thicknesses. Three pronounced vibronic absorption shoulders were found similar to pristine P3HT, implying the presence of ordered domain P3HT in the presence of TiO_2 nanorods. We have studied device performances as a function of the thickness of the active layer to achieve optimized performance (Fig. 6 inset). The devices reach their optimum performance at a layer thickness of ~100–150 nm. As the active layer film thickness further increases, the cell performances deteriorate. Open-circuit voltage (V_{oc}) has slightly differed around 0.55 V. A thicker film has greater photon absorption but the lower electric fields result in reduced charge separation efficiency and lower charge transport efficiency. The fill factor (FF) was found to have dropped significantly for a thicker layer (400 nm).

Fig. 7 presents the device tested under AM 1.5 illumination at an intensity of 100 mW/cm^2. The I–V characteristic of the device exhibits a J_{sc} of −2.97 mA/cm^2, a V_{oc} of 0.52 V and an FF of 0.54, yielding a power conversion efficiency of 0.83%. The external quantum efficiency (EQE) spectrum shows a maximum value of 28% under 500 nm is achieved (Fig. 7 inset). The power conversion

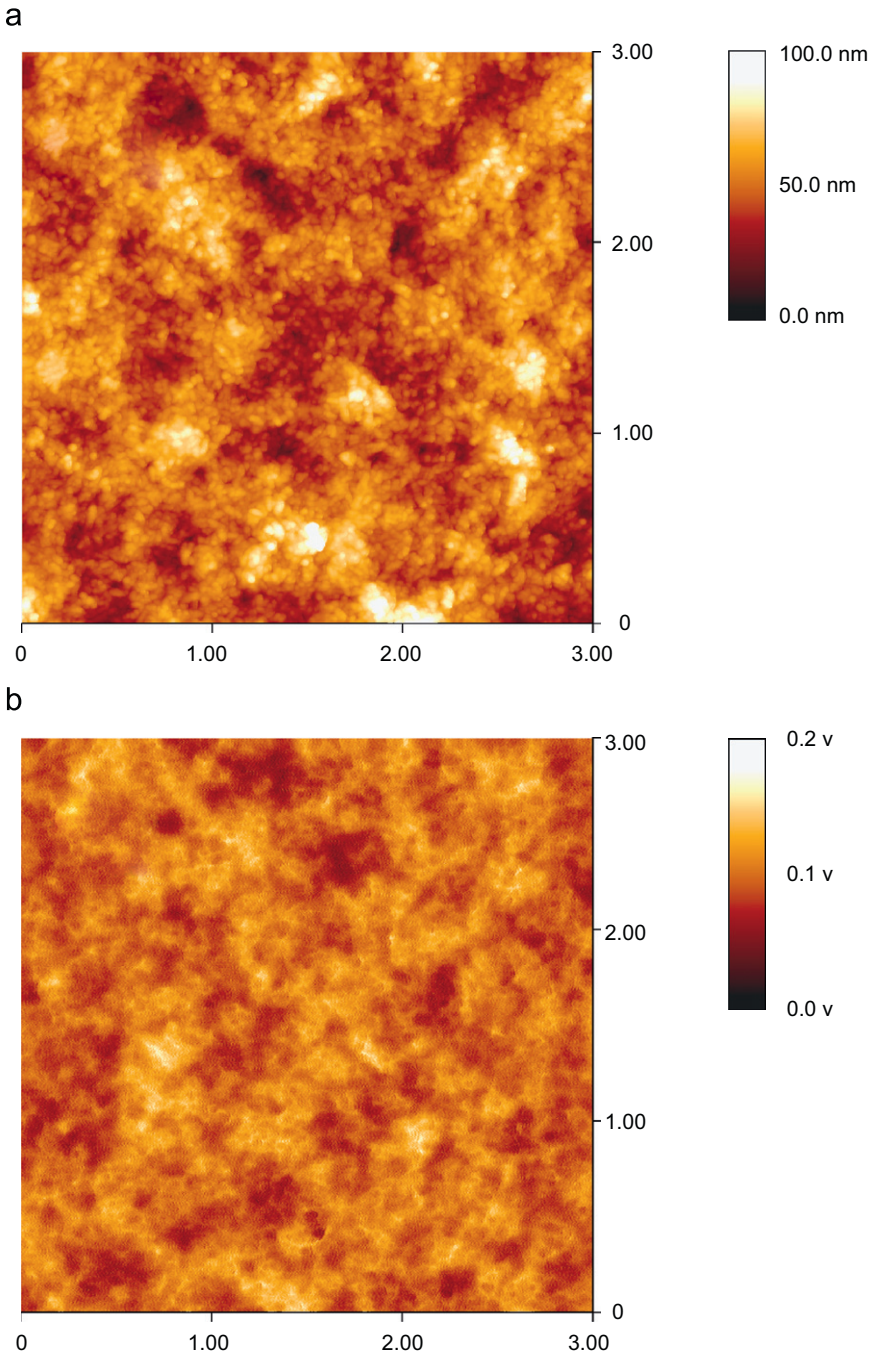

Fig. 9. (a) Topographic and (b) KPFM images of a spin-coated P3HT:TiO_2 blend from P3HT dissolved in TCB onto a conventional ITO/PEDOT:PSS substrate.

efficiency is about two times that of MEH-PPV:OLEA-TiO_2 nanorods solar cells [17]; this could be attributed to high hole mobility and efficient charge separation at the donor–acceptor interface.

It is worth noticing that the device EQE is <0.3 (Fig. 7 inset), but the fraction of light absorbed for a 100 nm hybrid film is $\sim$0.5 (Fig. 6) from 500 to 600 nm. Additionally, the absorbed value is higher in a device due to the reflection of the aluminum back electrode, which could cause the light to pass through the film twice. We considered the discrepancy between the large fraction of photons absorbed by a $\sim$100-nm-thick hybrid film and the lower EQE of photovoltaic cells. The current that a photovoltaic cell delivers corresponds to the number of created charges that are collected at the electrodes. This number depends on the fraction of photons absorbed (η_{abs}), the fraction of electron–hole pairs that are dissociated (η_{diss}), and finally the fraction of (separated) charges that reach the electrodes (η_{out}) determining the overall photocurrent efficiency

$$\eta_j = \eta_{abs} \times \eta_{diss} \times \eta_{out}$$

Several factors that might limit the devices efficiency are then discussed in the following paragraphs.

Fig. 8 shows the field dependence of the photocurrent (J_{PH}). The photocurrent was calculated by subtracting the dark current from the light current. The extracted photocurrent corresponds to the exciton dissociation probability and the recombination losses. The latter is related to the mean carrier drift length. As can be seen, J_{PH} is weakly dependent on the applied bias under reverse bias. This means that J_{PH} is weakly limited by the mobility of carriers [27]. If the carrier mobilities can be further improved, the device efficiency might be slightly enhanced.

We have used KPFM to study the blending of donor–acceptor in the dark. Fig. 9(a) shows the topography of a spin-coated P3HT:TiO_2 blend from P3HT dissolved in TCB onto a conventional ITO/PEDOT:PSS substrate. Fig. 9(b) reveals the surface potential of the same area of Fig. 9(a). A surface topography appears with aggregations in several tens of nanometers. Values of the work function of the hybrid material depend on the variation of mixing of the hybrid; the darker regions were interpreted as the TiO_2 nanorods region. For this region, work function is closer to the value of the work function of a pure TiO_2 nanorods thin film (data not shown). The potential distribution indicates that the hybrid is constituted by P3HT-rich, TiO_2-rich and interfacial phases. From the above results, we found bi-continuous phase formation but some of the donor or acceptor regions might exceed optimal phase segregation domain size as compared with the $\sim$10 nm donor–acceptor phase features found in optimized P3HT:[6,6]-phenyl C_{61} butyric acid methyl ester solar cells [1]. The features of large-phase segregation domains can possibly cause incomplete charge transfer, the losses might occur during exciton diffusion. We inferred that since J_{SC} or EQE is strongly related to the amount of excitons split at the interface, larger or random-scale phase separation seems to be one of the main factors that limit J_{SC} or EQE. The incomplete exciton quenching can be attributed to the low exciton diffusion length, which has been determined in a previous study on P3HT in combination with a flat bare TiO_2 film [26]. The exciton diffusion length extracted from their data is about only 3 nm, the low exciton diffusion length could be possibly due to the non-perfect electronic coupling between the P3HT and TiO_2 [28]. Therefore, one should be able to improve the device efficiency by further optimizing the hybrid material bi-continuous phase to a well-ordered defined domain size to decrease the exciton diffusion loss or using an appropriate surface modifier for better coupling between the P3HT and TiO_2 for increasing the exciton diffusion length [28].

4. Conclusion

The semiconductor oxide titanium dioxide nanorods were demonstrated, which can be incorporated into the P3HT, and solution-processed polymer-based solar cells could be made. The device performance was found to be critically dependent on material properties and processing conditions. And we proposed that by further optimizing the hybrid material bi-continuous phase, a further improved P3HT:TiO_2 nanorods solar cell performance can be obtained.

Acknowledgement

The authors thank the National Science Council of Republic of China (NSC95-3114-P-002-003-MY3) and the US Air Force (AOARD-07-4014) for financial support of this research.

References

[1] W. Ma, C. Yang, X. Gong, K. Lee, A.J. Heeger, Thermally stable, efficient polymer solar cells with nanoscale control of the interpenetrating network morphology, Adv. Funct. Mater. 15 (2005) 1617–1622.
[2] J.Y. Kim, K. Lee, N.E. Coates, D. Moses, T.-Q. Nguyen, M. Dante, A.J. Heeger, Efficient tandem polymer solar cells fabricated by all-solution processing, Science 317 (2007) 222–225.
[3] M. Granström, K. Petritsch, A.C. Arias, A. Lux, M.R. Andersson, R.H. Friend, Laminated fabrication of polymeric photovoltaic diodes, Nature 395 (1998) 257–260.
[4] W.U. Huynh, J.J. Dittmer, A.P. Alivisatos, Hybrid nanorod–polymer solar cells, Science 295 (2002) 2425–2427.
[5] P. Wang, A. Abrusci, H.M.P. Wong, M. Svensson, M.R. Andersson, N.C. Greenham, Photoinduced charge transfer and efficient solar energy conversion in a blend of a red polyfluorene copolymer with CdSe nanoparticles, Nanoletters 6 (2006) 1789–1793.
[6] W.J.E. Beek, M.M. Wienk, M. Kemerink, X. Yang, R.A.J. Janssen, Hybrid zinc oxide-conjugated polymer bulk heterojunction solar cells, J. Phys. Chem. B 109 (2005) 9505–9516.
[7] P. Ravirajan, D.D.C. Bradley, J. Nelson, S.A. Haque, J.R. Durrant, H.J.P. Smit, J.M. Kroon, Efficient charge collection in hybrid polymer/TiO_2 solar cells using poly(ethylenedioxythiophene)/polystyrene sulphonate as hole collector, Appl. Phys. Lett. 86 (2005) 143101-1-3.
[8] D.C. Olson, J. Piris, R.T. Collins, S.E. Shaheen, D.S. Ginley, Hybrid photovoltaic devices of polymer and ZnO nanofiber composites, Thin Solid Films 496 (2006) 26–29.
[9] D.C. Olson, S.E. Shaheen, M.S. White, W.J. Mitchell, M.F. AM van Hest, R.T. Collins, D.S. Ginley, Band-offset engineering for enhanced open-circuit voltage in polymer-oxide hybrid solar cells, Adv. Funct. Mater. 17 (2007) 264–269.
[10] J. Bouclé, P. Ravirajan, J. Nelson, Hybrid polymer–metal oxide thin films for photovoltaic applications, J. Mater. Chem. 30 (2007) 3141–3153.
[11] A.J. Breeze, Z. Schlesinger, S.A. Carter, P.J. Brock, Charge transport in TiO_2/MEH-PPV polymer photovoltaics, Phys. Rev. B 64 (2001) 125205-1-9.
[12] K.M. Coakley, M.D. McGehee, Photovoltaic cells made from conjugated polymers infiltrated into mesoporous titania, Appl. Phys. Lett. 83 (2003) 3380–3382.
[13] H. Wang, C.C. Oey, A.B. Djurišic, M.H. Xie, Y.H. Leung, K.K.Y. Man, W.K. Chan, A. Pandey, J.-M. Nunzi, P.C. Chui, Titania bicontinuous network structures for solar cell applications, Appl. Phys. Lett. 87 (2005) 023507-1-3.
[14] Q. Wei, K. Hirota, K. Tajima, K. Hashimoto, Design and synthesis of TiO_2 nanorod assemblies and their application for photovoltaic devices, Chem. Mater. 18 (2006) 5080–5087.
[15] Y.Y. Lin, C.W. Chen, T.H. Chu, W.F. Su, C.C. Lin, C.H. Ku, J.J. Wu, C.H. Chen, Nanostructured metal oxide/conjugated polymer hybrid solar cells by low temperature solution processes, J. Mater. Chem. 17 (2007) 4571–4576.
[16] C.Y. Kwong, W.C.H. Choy, A.B. Djurišic, P.C. Chui, K.W. Cheng, W.K. Chan, Poly(3-hexylthiophene): TiO_2 nanocomposites for solar cell applications, Nanotechnology 15 (2004) 1156–1161.
[17] T.-W. Zeng, Y.-Y. Lin, H.-H. Lo, C.-W. Chen, C.-H. Chen, S.-C. Liou, H.-Y. Huang, W.-F. Su, A large interconnecting network within hybrid MEH-PPV/TiO_2 nanorod photovoltaic devices, Nanotechnology 17 (2006) 5387–5392.
[18] A. Petrella, M. Tamborra, M.L. Curri, P. Cosma, M. Striccoli, P.D. Cozzoli, A. Agostiano, Colloidal TiO_2 nanocrystals/MEH-PPV nanocomposites: photo (electro)chemical study, J. Phys. Chem. B 109 (2005) 1554–1562.
[19] Y.-T. Lin, T.-W. Zeng, W.-Z. Lai, C.-W. Chen, Y.-Y. Lin, Y.-S. Chang, W.-F. Su, Efficient photoinduced charge transfer in TiO_2 nanorod/conjugated polymer hybrid materials, Nanotechnology 17 (2006) 5781–5785.
[20] H. Hoppe, T. Glatzel, M. Niggemann, A. Hinsch, M. Ch. Lux-Steiner, N.S. Sariciftci, Kelvin probe force microscopy study on conjugated polymer/fullerence bulk heterojunction organic solar cells, Nanoletters 5 (2005) 269–274.

[21] M. Chiesa, L. Bürgi, J.-S. Kim, R. Shikler, R.H. Friend, H. Sirringhaus, Correlation between surface photovoltage and blend morphology in polyfluorene-based photodiodes, Nanoletters 5 (2005) 559–563.
[22] P.D. Cozzoli, A. Kornowski, H. Weller, Low-temperature synthesis of soluble and processable organic-capped anatase TiO_2 nanorods, J. Am. Chem. Soc. 125 (2003) 14539–14548.
[23] N.C. Greenham, X. Peng, A.P. Alivisatos, Charge separation and transport in conjugated-polymer/semiconductor-nanocrystal composites studied by photoluminescence quenching and photoconductivity, Phys. Rev. B 54 (1996) 17628–17637.
[24] S.A. Choulis, Y. Kim, J. Nelson, D.D.C. Bradley, M. Giles, M. Shkunov, I. McCulloch, High ambipolar and balanced carrier mobility in regioregular poly(3-hexylthiophene), Appl. Phys. Lett. 85 (2004) 3890–3892.
[25] R.J. Kline, M.D. McGehee, E.N. Kadnikova, J. Liu, J.M.J. Fréchet, M.F. Toney, The dependence of regioregular poly(3-hexylthiophene) film morphology and field effect mobility on molecular weight, Macromolecule 38 (2005) 3312–3319.
[26] Y. Kim, S. Cook, S.M. Tuladhar, S.A. Choulis, J. Nelson, J.R. Durrant, D.D.C. Bradley, M. Giles, I. Mcculloch, C.-S. Ha, M. Ree, A strong regioregularity effect in self-organizing conjugated polymer films and high-efficiency polythiophene: fullerene solar cells, Nat. Mater. 5 (2006) 197–203.
[27] W.U. Huynh, J.J. Dittmer, N. Teclemariam, D.J. Milliron, A.P. Alivisatos, K.W.J. Barnham, Charge transport in hybrid nanorod-polymer composite photovoltaic cells, Phys. Rev. B 67 (2003) 115326-1-12.
[28] C. Goh, S.R. Scully, M.D. McGehee, Effects of molecular interface modification in hybrid organic-inorganic photovoltaic cells, J. Appl. Phys. 101 (2007) 114503-1-12.